Coordination Chemistry Reviews, 120 (1992) 361–387
Elsevier Science Publishers B.V., Amsterdam

Structural flexibility and bonding capabilities of the ligand np_3 toward the transition metals

Carlo Mealli, Carlo A. Ghilardi and Annabella Orlandini
Istituto per lo Studio della Stereochimica ed Energetica dei Composti di Coordinazione, C.N.R., Via J. Nardi 39, 50132 Florence (Italy)

(Received 6 November 1991)

CONTENTS

A. INTRODUCTION

An important aspect of modern organometallic chemistry is connected with the residual bonding capabilities that a specific metal fragment can exert toward organic substrates. It is indisputable that some successful chemists have tied their name to a specific molecular fragment able to promote the reactivity of organic substrates, a good example being $(CO)Cl(Ph_3)_2Ir$, better known as Vaska's compound. [1].

Another remarkable example of a fragment supporting a variety of chemical behaviours is $(np_3)M$ in which np_3 is the ligand tris(2-diphenyl-phosphinoethyl)-amine, $N(CH_2CH_2PPh_2)_3$ [2].

The latter fragment characterizes a great part of the work performed over 20 years by the florentine school founded by Prof. Luigi Sacconi. Today, the scientific inheritance of np_3–metal chemistry remains firmly in the hands of the pupils of Sacconi, as indicated by the fact that all of the 60 structures containing the fragment and present in the Cambridge Structural Database (CSD) [3] have been determined in the laboratories at Florence.

To be a successful precursor of relevant chemical reactions, a specific metal fragment must be unsaturated, both coordinatively and electronically, and must also have good stability and a sufficiently long lifetime. These features are often found in np_3–metal chemistry. Moreover, the relative ease with which these fragments undergo structural rearrangements reflects important compositional changes of the frontier MOs. The latter can vary both in energy and hybridization and the metal can accept coligands in different coordination modes and number. Sometimes, the metal fragment promotes the reactivity of incoming organic substrates. The latter points have been made clear by the richness of the experimental chemistry performed over the years on the $(np_3)M$ systems as well as by the large amount of collected X-ray structural data.

In this paper, we summarize the various bonding capabilities of the ligand np_3. The subtle interplay between geometric and electronic factors that govern the chemistry of these metal complexes is illustrated in the light of the experimental and interpretational work performed to date. Moreover, we try to offer a viewpoint of the np_3 chemistry unified under the principles of MO theory and the analysis of the fragment orbital interactions (see Appendix).

B. GENERAL ASPECTS OF THE np_3–METAL BONDING

Given the presence of four donor atoms and the equivalence of the three arms departing from the central amine nitrogen atom, the ligand np_3 can potentially wrap metals in an umbrella-like fashion. The resulting fragment most often adopts a trigonal pyramidal geometry (TP) with one axial M–N and three equatorial M–P bonds (see I). The threefold symmetry is maintained even when the M–N bond, more labile than the three M–P bonds, elongates significantly (up to ca. 3.5 Å).

Given the chained connectivity between amine and phosphines, the M–N elongation is accompanied by a displacement of the phosphorus atoms away from the equatorial plane and toward the side of the central amine ligand. When any residual metal–amine interaction is lost, the TP chromophore NP_3M has converted into a P_3M pyramid, as shown in II. Importantly, the overall rearrangement has little cost in terms of conformational energy as it seems to be mainly controlled by an interplay of torsions about the single bonds forming N–C–C–P chains.

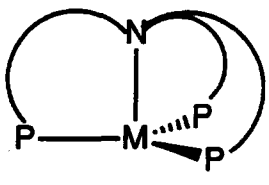

I

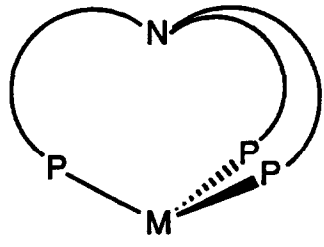

II

The plot in Fig. 1, constructed from 40 structures with approximate threefold symmetry, shows a good linear relationship between the M–N distance and the average N–M–P angle (a measure of the out-of plane displacement of the P atoms).

Apart from three complexes (black squares) characterized as pure $(np_3)M$ fragments with no extra coligand (see Sect. F), three structural subsets can be easily identified in the plot:

(i) The structures at the bottom right of the plot are characterized by an $M–N_{amine}$ single bond. A fifth donor completes a local trigonal bipyramidal coordination at the metal (TBP) (Table 1).

(ii) In the pseudo-tetrahedral structures (PT), at the top left of the plot (see Table 2), the M–N bonding interaction has practically vanished. A repulsion between axial lone pairs would probably sweep away the amine but the connectivity requirements of np_3 fix a maximum M–N distance of ca. 3.5 Å with a correlated N–M–P angle of ca. 63°. Notice that, at the ideal angular value of 55° (corresponding to P–M–P angles of ca. 90°), the fragment $(np_3)M$ would contain a P_3M chromophore in a regular hemioctahedral geometry. Since the latter limit is not reached, the metal frontier orbitals (especially those of d_π type) cannot attain the highest possible degree of hybridization typical of other C_{3v} fragments of the L_3M type [32], e.g. those formed with triphos $(CH_3(CH_2PPh_2)_3)$, another classic ligand in this laboratory. Hence, there are some subtle differences between the chemistry of the two fragments.

(iii) An intermediate group of five paramagnetic structures, trigonally elongated (TE), lies in the central part of the plot with an M–N range of 2.63–2.73 Å (see Table 3). In spite of different metal electron counts (d^5–d^7), the five cases are similar because they contain more than one unpaired electron, one of which is in a frontier MO with overall axial $(N–M–L_{ax})$ antibonding character (see Sect. E). The latter MO is empty in the complexes of the group (i) so that the two trans-axial bonds can

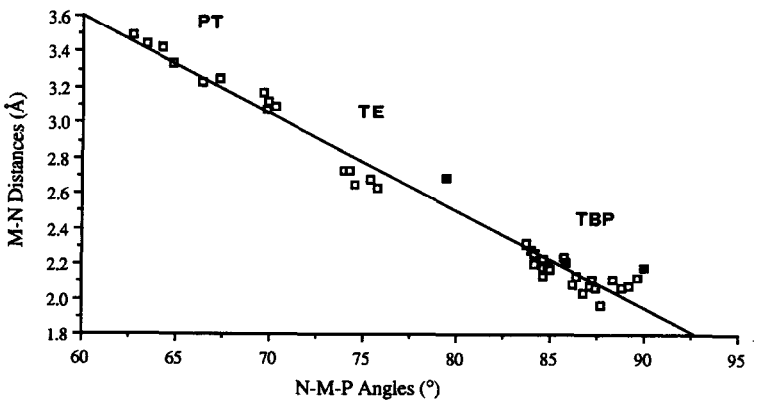

Fig. 1. A plot correlating the M–N distance with the average angle N–M–P in 40 structures containing the np_3 ligand and having approximate C_{3v} symmetry. The black squares refer to the three known cases in which the complex has the simplest formula $(np_3)M$, i.e. no other coligand is present.

TABLE 1

Diamagnetic complexes containing electronically saturated (18e) metal centres in local trigonal bipyramidal (TBP) geometry

Compound	M–N	M–P (range)	P–M–P (range)	N–M–P (range)	Ref.
$[(np_3)Co(CS)]^+$	2.03(1)	2.15(2)–2.23(3)	115.1(8)–124.3(8)	85(2)–89(2)	4
$[(np_3)Co(CO)]^+$	2.06(2)	2.17(1)–2.19(1)	118.2(4)–121.7(3)	86.9(7)–88.4(7)	5
$[(np_3)Co(H)]$	2.067(5)	2.110(3)–2.118(3)	115.8(1)–124.1(1)	88.9(2)–89.7(2)	6
$[(np_3)Co(Hg_2)Co(np_3)]$	2.11(4)	2.11(1)–2.16(1)	119.1(6)–121.1(6)	87(1)–89(1)	7
$[(np_3)Ni(Cl)]^+$	1.97(1)	2.194(5)–2.298(4)	114.0(2)–126.7(2)	86.0(3)–89.5(3)	8
$[(np_3)Ni(H)]^+$	2.06(2)	2.197(5)–2.214(5)	119.6(2)–120.8(2)	88.1(4)–89.4(4)	9
$[(np_3)Ni(SO_3Et)]^+$	2.070(8)	2.279(3)–2.335(3)	113.8(1)–124.1(1)	86.8(2)–87.4(2)	10
$[(np_3)Ni(SnPh_3)]^+$	2.08(5)	2.25(2)–2.30(2)	116.0(7)–122.0(7)	85(1)–90(1)	11
$[(np_3)Ni(CH_3)]^+$	2.11(1)	2.216(6)–2.250(5)	117.1(2)–122.8(2)	86.5(4)–87.9(4)	12
$[(np_3)Ni(I)]^+$	2.13(4)	2.22(1)	120.0(5)	89.6(5)	13
$[(np_3)Ni(CO_2Et)]^+$	2.13(1)	2.242(3)–2.340(3)	113.8(1)–124.6(1)	86.2(3)–86.7(3)	14
$[(np_3)Ni(COCH_3)]^+$	2.31(3)	2.27(1)–2.31(2)	113.8(6)–126.2(6)	82.2(8)–84.4(8)	15
$[(np_3)Ni(SO_2)]$	2.31(1)	2.248(2)	118.83(5)	83.75(7)	16
$[(np_3)Pd(CH_3)]^+$	2.23(2)	2.357(4)	119.1(2)	84.6(1)	17
$[(np_3)Pt(CH_2Cl)]^+$	2.18(2)	2.343(9)–2.399(9)	117.1(3)–121.9(3)	83.5(7)–86.0(7)	18
$[(np_3)Pt(PHEt_2)]^+$	2.196(2)	2.376(4)–2.409(3)	117.5(1)–120.0(1)	83.9(2)–84.4(3)	19
$[(np_3)Pt(HgCH_3)]^+$	2.23(1)	2.301(5)–2.320(5)	116.7(2)–121.1(2)	85.3(4)–86.3(4)	20
$[(np_3)Pt(AsPh_2)]^+$	2.276(7)	2.312(3)–2.388(3)	109.8(1)–124.6(1)	83.3(3)–84.6(2)	21
$[(np_3)Rh(Te_2)Rh(np_3)]$	2.190(6)	2.288(2)–2.319(2)	112.3(1)–123.0(1)	84.5(2)–85.3(2)	22

TABLE 2

Complexes containing metal centres in local pseudo-tetrahedral (PT) geometry

Compound	M–N	M–P (range)	P–M–P (range)	N–M–P (range)	Ref.
$[(np_3)Co(Br)]$	3.34(1)	2.279(5)–2.295(4)	102.7(2)–103.6(2)	64.2(3)–65.2(3)	23
$[(np_3)Co(\eta^3\text{-}P_3)]$	3.42(1)	2.310(5)–2.325(5)	102.1(1)–103.3(2)	64.2(3)–64.5(3)	24
$[(np_3)Co(\eta^2\text{-}SCNPh)]$	3.44(1)	2.269(4)–2.303(4)	100.2(2)–103.5(2)	62.3(4)–64.8(4)	25
$[(np_3)CoSCo(np_3)]$	3.485(8)	2.285(9)	100.7(2)	62.7(3)	26
$[(np_3)Ni(\eta^1\text{-}P_4)]$	3.09(2)	1.99(1)	109.3(7)	70(1)	27
$[(np_3)Ni(P_4Se_3)]$	3.124(8)	2.246(3)	108.9(1)	70.0(2)	28
$[(np_3)Ni(P_4S_3)]$	3.166(8)	2.245(3)	108.5(1)	69.6(2)	29
$[(np_3)Ni(NO)]^+$	3.23(1)	2.280(5)–2.302(6)	103.1(2)–106.5(2)	65.8(5)–66.8(5)	30
$[(np_3)Ni(CO)]$	3.25(1)	2.205(4)–2.223(3)	105.8(1)–106.3(1)	66.9(2)–67.7(2)	5
$[(np_3)Hg(I)]^+$	3.07(1)	2.523(9)–2.548(8)	107.7(3)–109.9(3)	69.4(5)–70.4(5)	31

TABLE 3
High-spin d^5–d^7 $[(np_3)ML]^+$ complexes with trigonally elongated (TE) geometry

Compound		M–N	M–P (range)	P–M–P (range)	N–M–P (range)	Ref.
$[(np_3)Mn(I)]^+$	d^5	2.634(9)	2.548(3)–2.567(4)	113.0(1)–114.9(1)	75.1(2)–76.2(2)	33
$[(np_3)Fe(Br)]^+$	d^6	2.65(2)	2.427(6)–2.445(7)	110.1(2)–116.4(2)	73.4(4)–75.9(4)	34
$[(np_3)Co(Cl)]^+$	d^7	2.68(1)	2.355(4)–2.377(4)	110.1(1)–118.4(2)	74.6(2)–76.1(2)	35
$[(np_3)Co(Br)]^+$	d^7	2.73(1)	2.355(7)–2.402(7)	110.2(2)–114.6(2)	73.1(3)–74.8(3)	36
$[(np_3)Co(I)]^{+a}$	d^7	2.73(1)	2.351(4)–2.375(4)	111.7(2)–115.3(2)	74.2(3)–74.4(2)	36

[a] BPh_4^- as counter-ion.

be assigned a bond order of 1. By contrast, two electrons in that orbital would correspond to the previous case (ii) where the N and M lone pairs repel each other (bond order = 0). Evidently, for the five structures (iii), the M–N bond order is fractional (formally = 0.5).

Finally, two additional categories of $(np_3)M$ fragments (not included in the plot of Fig. 1) must be pointed out in terms of their structural features:

(iv) In the structures reported in Table 4, the $(np_3)M$ fragment has lost threefold symmetry. Generally, this occurs simply through the opening of one of the three P–M–P angles from 120° toward 180°. At the latter limit, the former TP fragment is transformed into a classic butterfly fragment of the type L_4M with pseudo C_{2v} symmetry (actual C_s) [32] (see **III**). The geometrical distortion offers new bonding and reaction capabilities to the fragment $(np_3)M$ ($M = d^8$). Depending on the nature of the metal and of the coligand, the degree of TP/butterfly interconversion can alternatively favour significant organometallic processes such as oxidative addition or reductive elimination. This aspect will be discussed in Sect. I.

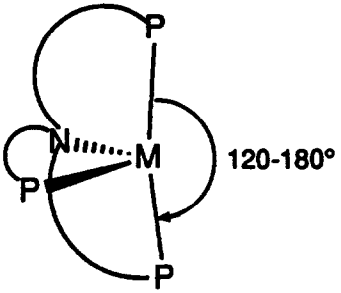

III

(v) Occasionally, the overall wrapping mode of np_3 about a single metal is lost. For example, the np_3 arms can coordinate more metals, e.g. $[(np_3)\{Rh(C_5H_5)\}_3Cl_5)]^+$ [41] and $[Pt(\mu\text{-}np_3)(\mu\text{-}PEt_2)Pt(PPh_3)]^+$ [42] (**IV**).

Alternatively, one of the arms remains uncoordinated, e.g. $[(np_3)Ni(CH{=}CHC(O)OEt)]^+$ [39] (**V**) and, in some cases, the free phosphine is even subject to chemical

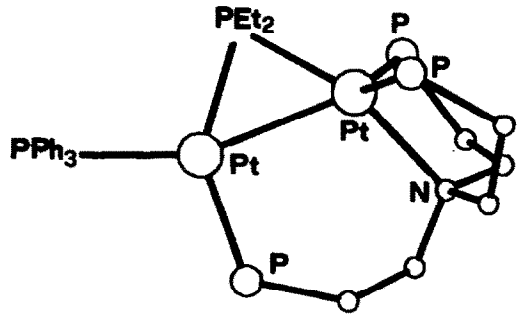

IV

TABLE 4

Low-spin d^7 $[(np_3)ML]^+$ complexes with distorted geometry (breakdown of the C_{3v} symmetry)

Compound	M–N	M–P (range)	P–M–P (range)	N–M–P (range)	Ref.
$[(np_3)Co(I)]^+$ [a]	2.12(2)	2.229(8)–2.279(8)	97.3(3)–159.8(3)	84.9(6)–87.2(6)	37
$[(np_3)Co(SCH_3)]^+$	2.13(1)	2.245(5)–2.289(5)	111.8(2)–133.5(2)	84.3(3)–84.9(3)	38
$[(np_3)CoC(CO_2Et)CH_2]^+$	2.16(1)	2.270(4)–2.340(4)	102.6(2)–148.8(2)	84.7(3)–85.9(3)	39
$[(np_3)Co(SO_3Et)]^+$	2.17(1)	2.275(6)–2.318(6)	112.2(2)–130.5(2)	84.5(3)–85.6(3)	40

[a] I^- as counter-ion.

attack with in situ formation of a phosphine-oxide group (e.g. $[(np_3O)Co(NO)_2]^+$ [43] (VI). Given the serendipity of these compounds, neither their structural features nor the causes that push the ligand np_3 to adopt unusual coordination modes will be analyzed in detail.

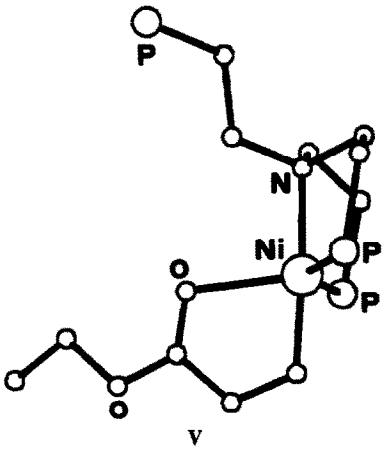

V

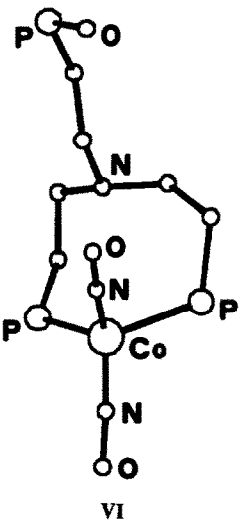

VI

C. DIAMAGNETIC TRIGONAL BIPYRAMIDAL (TBP) COMPLEXES OF THE TYPE $(np_3)ML$ [$M = d^8$]

Since np_3 is potentially a four lone pair donor, the presence of a coligand donating two additional electrons satisfies the 18 electron rule for a d^8 metal atom. When the five-coordination field was initially explored, Sacconi designed the tripod-like ligand np_3 to obtain stable TBP complexes. In Fig. 1, complexes belonging to this category (Table 1) are scattered along the least-square straight line in the bottom right portion of the plot. Whenever different metal ions are involved (Co(I), Ni(II), Pd(II), Pt(II), Rh(I)), their radii are thought to cause different M–N elongations. However, for a unique metal centre, the trans influence between the amine and the axial coligand becomes important. As an example, the Ni–N distances vary by as much as 1.97(1) Å in $[(np_3)NiCl]^+$ [8] to 2.31(1) Å in $(np_3)Ni(SO_2)$ [16].

Trans influence has long been debated in the literature [44]; still we wish to point out the following ideas derivable from qualitative MO theory and supported by EHMO calculations with the fragment orbital analysis [45]. The arguments are also helpful to recall basic aspects of five coordination [46] that may be applied to metal–ligand bonding in $(np_3)M$ complexes.

Figure 2 shows the interaction between the TP model of $[(np_3)Ni]^{2+}$ and a two-electron donor ligand trans to nitrogen, a hydride in the most simple case. On the left, the FMOs of the C_{3v} metal fragment can be described as follows. The overall equatorial Ni–P bonding involves mostly the metal s, p_x and p_y orbitals. The latter, no longer available for bonding, do not appear in Fig. 2. Four of the five d orbitals are essentially non-bonding (xz, yz in 1e and xy, x^2-y^2 in 2e). The z^2 and p_z orbitals together with the amine lone pair generate the three FMOs of axial symmetry a_1. The lowest $1a_1$ is essentially an M–N σ-bonding combination which involves the metal z^2 orbital. In the first approximation, $2a_1$ is the z^2–N antibonding counterpart, although the effect is reduced by the mixing of p_z. Such a hybridization develops the σ lobe toward the trans axial position, as indicated by a CACAO drawing [47] of $2a_1$ (Fig. 2.) The latter FMO, which is empty for a d^8 metal, receives electron density from the hydride H_{1s} orbital on the right of the figure. This activates Ni–H σ-bonding together with partial Ni–N antibonding.

Whenever different coligands are involved, the smaller the energy gap between the σ-hybrid of L_{ax} and the $2a_1$ FMO, the larger is the strengthening and the weakening of the M–L_{ax} and M–N bonds, respectively. Both effects are, at least initially, enhanced with decreasing electronegativity of L_{ax}. When the energy of the L_{ax} σ-hybrid becomes higher than that of the $2a_1$ FMO, the two electrons that allow M–L_{ax} bonding remain preferentially localized on the side of the metal on the basis of simple perturbation theory principles [48]. Thus, the donor–acceptor relationship is inverted and the complex is better described as formed by a d^{10} metal back-donating into an acidic (or σ acceptor) ligand. Most likely this picture is appropriate for a complex such as $[(np_3)Ni(SnPh_3)]^+$ [11] (**VII**), where the $2a_1$ FMO is ca. 2 eV lower that the σ-$SnPh_3$.

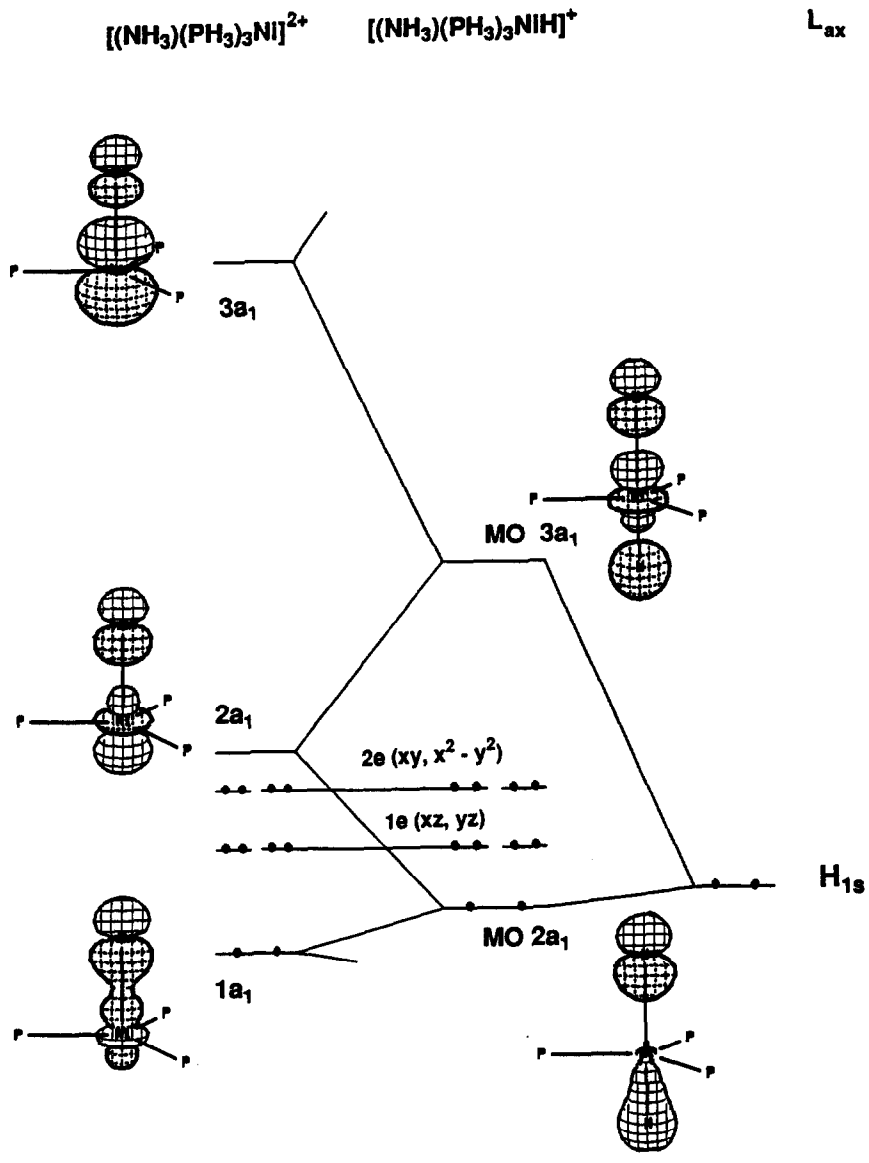

Fig. 2. Diagram for the interaction between a model of the $[(np_3)Ni]^{2+}$ fragment and the hydride coligand in C_{3v} symmetry.

Analogously, the presence of a very electropositive element such as Hg at one TBP apex (e.g. in the dimer $[(np_3)Co–Hg_2–Co(np_3)]$ [7] (**VIII**) and in the cation $[(np_3)Pt(HgCH_3)]^+$ [20]) is consistent with the transition metal acting as the σ donor.

Other cases appear dubious, e.g. the complex $(np_3)Ni(SO_2)$ [16] (**IX**), where

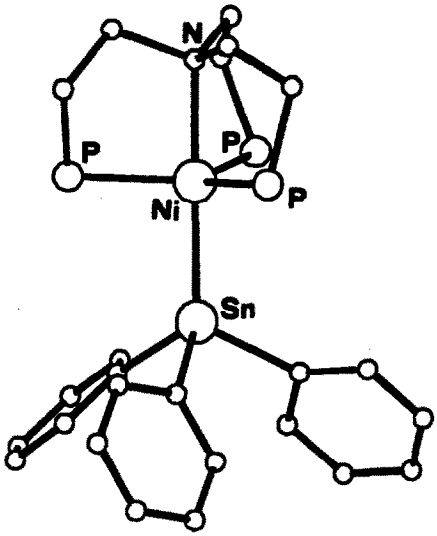

VII

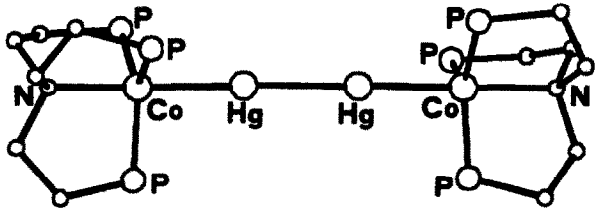

VIII

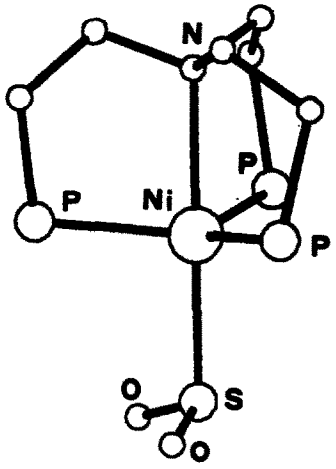

IX

the bending SO_2 would suggest the presence of the SO_2^{2-} dianion [49]. On the other hand, the adduct is experimentally formed from the interaction of two neutral molecular pieces such as gaseous SO_2 and the complex $(np_3)Ni(0)$ [6(a),50]. Moreover, since the calculated M–N overlap population decreases monotonously with increasing electropositivity of the trans coligand, the longest M–N distance found (2.31(1) Å) could suggest that, in this case also, the metal acts as a σ donor.

In conclusion, the order in which the M–N distances increase in Table 1 for a given metal seems to be related to the order of increasing electropositivity of the σ-hybrid coligand. A very electronegative ligand, such as chloride, should produce

only a minor elongation of the M–N bond. The relation trans influent/trans influenced is even inverted in the latter case (in the $2a_1$ MO, the M–Cl antibonding character prevails over that of M–N). Significantly, in the structure $[(np_3)NiCl]BPh_4$ [8], the Ni–N bond is the shortest observed for np_3 complexes (1.97(1) Å). The trans influence on the M–Cl bond is more difficult to evaluate since comparisons should be made within a series of structures having different trans ligands. Interestingly, a search in the CSD file [3] shows that, in TBP and square planar Ni(II) diamagnetic complexes, the average Ni–Cl bond is elongated by ca. 0.04 Å when the trans-amine σ donor is substituted by the stronger phosphine analog.

D. PARAMAGNETIC LOW-SPIN COMPLEXES OF THE TYPE $(np_3)ML$ [$M = d^7$]

In Table 4 are reported four complexes that can be formally considered to be derived from the stable class of TBP 18e complexes upon the removal of a single electron. With reference to the typical TBP pattern (centre of Fig. 2), the missing electron could originally populate one member of the degenerate 2e set (xy, x^2-y^2). Under these circumstances, the 17e system is Jahn–Teller unstable and a more or less pronounced distortion from threefold symmetry is observed in the crystal structures. The effect is most enhanced in the complex cation $[(np_3)CoI]I$ (**X**) [37] where one P–Co–P angle is as large as 159.8(3)°. As shown on the right of Fig. 3, the breakdown of C_{3v} symmetry splits the components of both 1e and 2e. Regarding 2e, xy drops in energy (the two rearranging phospine ligands point more and more towards the node of this orbital); the opposite is true for x^2-y^2. In going toward SQ geometry, x^2-y^2 (2a′) moves up and mixes heavily with the higher z^2-based level (3a′) and eventually the characters are switched. A similar avoided crossing will be helpful to understand some reactivity trends of d^8-$(np_3)M$ fragments (see final Sect. I). Concerning the present complexes, a 17-electron species is stable as soon as the separation (ΔE) between the two members of the 2e set becomes sufficiently large. The avoided crossing does not necessarily take place.

E. TRIGONALLY ELONGATED (TE) HIGH-SPIN COMPLEXES OF THE TYPE $(np_3)ML$ ($M = d^5$–d^8)

The cationic species $[(np_3)CoI]^+$ is not only interesting for the distortional aspect discussed above, but it also represents a remarkable example of spin isomerism. In solution, a temperature-dependent equilibrium between doublet and quadruplet ground states was detected. By using the counterion BPh_4^- [36] in place of I^- [37], the high-spin isomer could be isolated and structurally characterized (**XI**). Here, the cation has an elongated pseudo-C_{3v} geometry like the other TE structures in the centre of Fig. 1 and listed in Table 3. For this reason, it is convenient first to illustrate the general features of these few complexes having a variable electron count (d^5–d^7).

The evolution of the MOs for the trigonal elongation of a TBP species (left side of Fig. 3) rationalizes stability and similarity of the five TE structures. In the

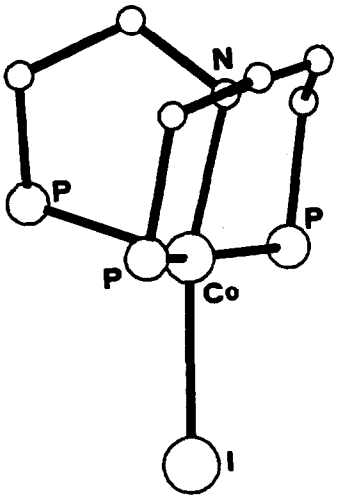

X

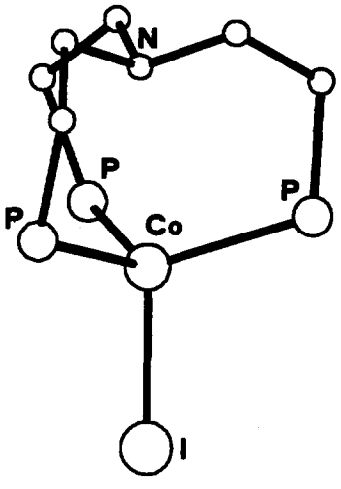

XI

recently characterized $[(np_3)MnI]^{1+}$ species [33], the five d-base levels 1e, 2e, $3a_1$ are singly occupied. While the two sets 1e and 2e are essentially non-bonding, the MO $3a_1$ is both M–N and M–L_{ax} antibonding (σ^*). Even a single electron can stretch both the trans-axial bonds of TBP, but in particular the amine is most influenced. Because of the reduced M–N bonding interaction, the $3a_1$ MO drops in energy and approaches the 2e levels (xy, x^2-y^2 based). Reasonably, the TE structure is consistent with a small $3a_1$/2e gap, a feature that in turn favours the highest spin multiplicity.

An additional electron with respect to $[(np_3)MnI]^{1+}$, as in the complex

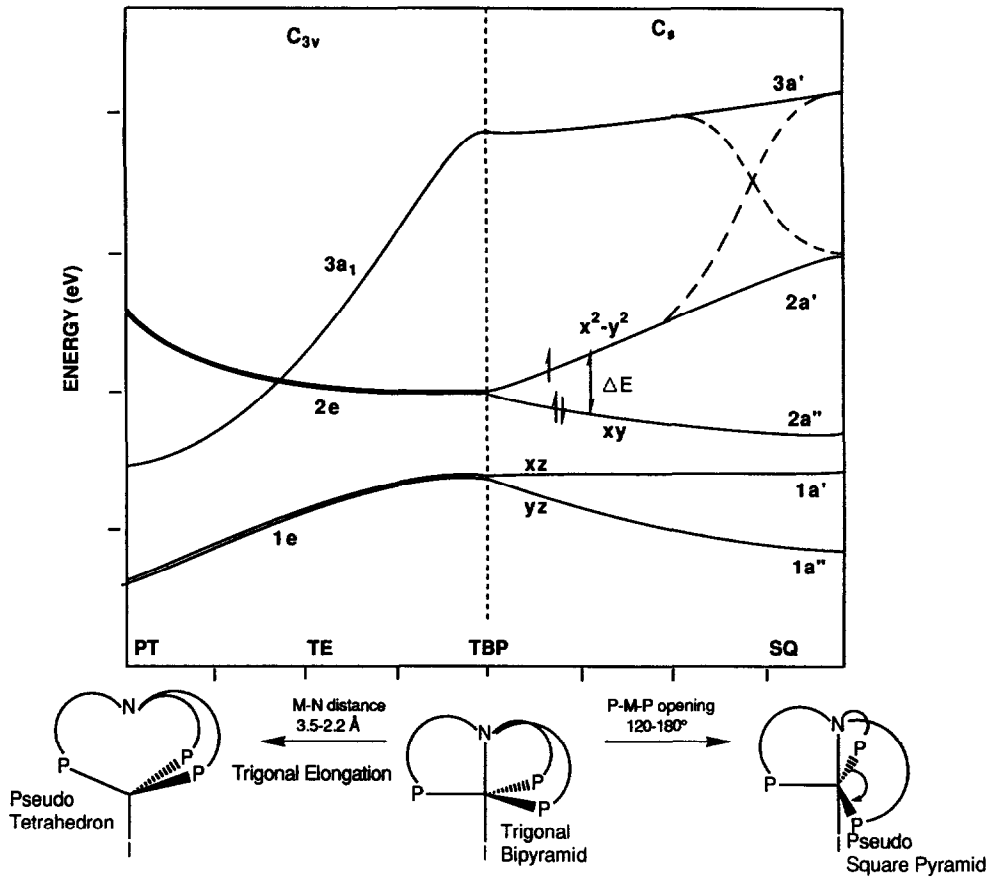

Fig. 3. A Walsh diagram showing the evolution of the frontier MOs of a model of $[(np_3)CoI]^+$. Two distinct structural variations are described: (i) distortion of the TBP structure toward a square pyramid (to the right of the vertical broken line). The governing parameter is one P–M–P angle (range 120–180°). (ii) Elongation of the TBP structure toward a pseudo-tetrahedron (to the left of the vertical broken line). Two parameters are changed simultaneously, namely the M–N distance (range 2.0–3.5 Å) and the average N–M–P angle (range 90–60°).

$[(np_3)FeBr]^+$ [34], $M = d^6$, does not alter the main geometrical features as it enters the lower essentially non-bonding 1e set. Even a seventh electron is still consistent with the TE structure because, in this case, the inert 1e level would be electronically saturated.

The geometry at which the crossing between $3a_1$ and 2e occurs is a variable that seems to depend on the nature of the metal as well as on that of the fifth donor L_{ax}. All three d^7 complexes $[(np_3)CoX]^+$, X = Cl [35], Br [36], I [36] can have a quadruplet state and TE structure. However, only if the donor strength of the axial ligand is sufficient to keep $3a_1$ above 2e (Fig. 3), as may be the case for iodide, can the formation of a low-spin isomer be explained. Small variations of the temperature as well as of the surrounding force field (packing forces included) can start the process

of spin pairing. An increased axial field quickly destabilizes the $3a_1$ in going toward TBP (notice the steep slope of $3a_1$ in Fig. 3). Recall, however, that the TBP geometry is metastable for a d^7 low-spin metal and eventually the complex is distorted toward SQ.

Even if no TE complex of d^8 metals is known, the MO trends (left side of Fig. 3) account for the existence of $(np_3)MX$ complexes other than diamagnetic. Only a strong axial field largely destabilizes $3a_1$ and favours the formation of the 18e TBP complexes. Conversely, if the $2e/3a_1$ gap is not sufficiently large, the configuration $(1e)^4(2e)^3(3a_1)^1$ is, in principle, possible but the complex would be subject to geometric distortions which are not easily predictable. On the other hand, a weak axial field allows $3a_1$ to lie below 2e, hence, the configuration $(1e)^4(3a_1)^2(2e)^2$ becomes favoured. The latter situation is appropriate for a Co(I) complex having a triplet ground state, namely $[(np_3)CoBr]$ (**XII**) [23].

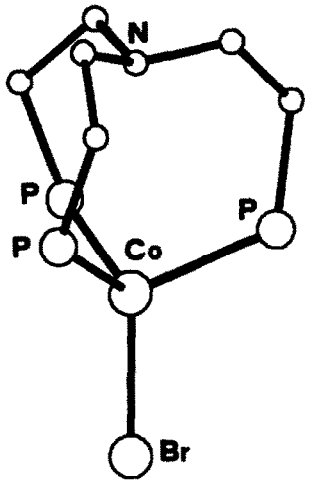

XII

The long Co–N distance of 3.34(1) Å (typical of diamagnetic PT complexes discussed in Sect. H) indicates the presence of two electrons in the M–N $3a_1$ antibonding level which triggers strong repulsion between the axial lone pairs.

As pointed out elsewhere [23], the conversion between high-spin and diamagnetic 18e complexes seems precluded by the presence of the crossing of levels, a sort of symmetry-imposed barrier. Importantly, no such problem seems to exist for the interconversion of low-spin/high-spin d^7 complexes such as $[(np_3)CoI]^+$. This observation suggests that, in addition to control evidently exerted by geometry, the nature of the metal and of the coligand represents an even more subtle factor to consider. Thus, it is remarkable that d^8 metals such as Ni(II) and Co(I) can give rise to quite different derivatives. Complexes of the former ion are invariably diamagnetic with TBP structure. The strength of the coligand is instead decisive for the ground state of the Co(I) species. Only a strong σ donor (e.g. H^- or CN^-) can stabilize the TBP

structure, whereas a triplet ground state is obtained with the weaker halide ligands (e.g. $(np_3)CoBr$) or with no coligand at all. The latter is the case for the complex $[(np_3)Co]^+$ [9] discussed in the next section.

F. TRIGONAL PYRAMIDAL (TP) $(np_3)M$ COMPLEXES WITH NO COLIGAND

The triplet ground state of $[(np_3)Co]^+$ [9] is consistent with two unpaired electrons in the highest 2e set and with a fully populated z^2-based level ($2a_1$). Even if the latter MO maintains partial Co–N antibonding character, the structure in **XIII** is close to a somewhat elongated trigonal pyramid. In fact, the Co–N distance of 2.21(2) Å is a ca. 0.3 Å longer than the sum of the covalent radii. The relatively weak M–N repulsion is consistent with significant mixing of p_z into z^2, which redirects the large axial lobe (hence the two electrons in it) in the direction of the fifth missing ligand (see the $2a_1$ FMO in Fig. 2.). The arguments also apply to the TP complex $(np_3)Ni(0)$ (**XIV**) [6(a), 50] where the Ni–N distance (2.18(7) Å) is very close to that of Co–N. The latter Ni(0) species is obtainable via chemical reduction of Ni(II) salts in the presence of np_3 and contains a basic metal. The acquired reducing power is attributable to the axial lone pair ($2a_1$ FMO) now having HOMO character (at variance with $[(np_3)Co]^+$).

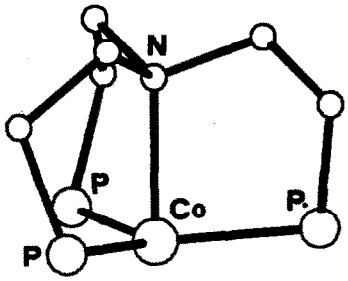

XIII

In addition to $[(np_3)Co]^+$ and $(np_3)Ni(0)$, a third case is known in which np_3 is accompanied by no other ligand, namely the complex $(np_3)Pd(0)$ (**XV**) [51]. Structural data for the three complexes are summarized in Table 5.

Although isoelectronic with $(np_3)Ni(0)$, the $(np_3)Pd(0)$ complex has a surprisingly elongated conformation similar to the TE complexes of Sect. E (Pd–N) = (2.69(2) Å). However, the causes for the elongation are different in this case. Given the increasing gap between d and p atomic orbitals down the triad Ni, Pd, Pt, the mixing of p_z into z^2 becomes increasingly difficult. Without suitable rehybridization, the electron density in the $2a_1$ FMO cannot be redirected away from the amine so that the four-electron repulsion between the M and N atoms remains quite active. As the Pd–N bond is elongated, $2a_1$ drops lower that the 2e set (see Fig. 4). Since the crossing between filled levels is allowed, two almost equivalent energy minima are calculated for the TE and TP structures, respectively. The energy barrier, calcu-

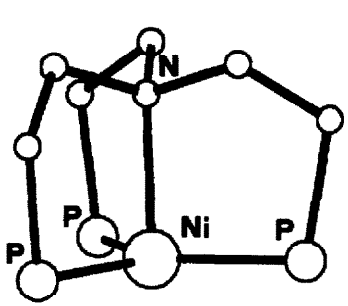

XIV

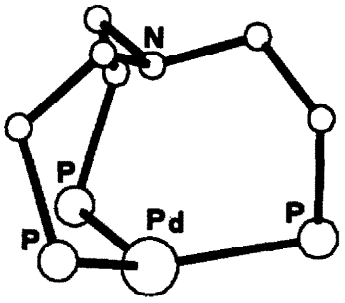

XV

TABLE 5

[$(np_3)M^n$ ($n = 0, +1$) complexes having trigonal pyramidal (TP) geometry with no coligand

Compound	M–N	M–P (range)	P–M–P (range)	N–M–P (range)	Ref.
[(np_3)Ni]	2.178(7)	2.117(3)–2.121(3)	115.4(1)–124.5(1)	89.4(1)–90.6(2)	6a, 50
[(np_3)Co]$^+$	2.21(2)	2.246(7)–2.267(7)	114.8(3)–126.4(3)	84.9(5)–87.2(6)	9
[(np_3)Pd]	2.69(2)	2.299(5)	116.7(1)	79.4(1)	17, 51

lated at the EHMO level, is very low (ca. 0.1 eV) and the TE structure may be attributable to a solid state effect. In solution, TP and TE isomers may have practically equal opportunities to exist. Importantly, the easy access to the structure of type **XIV** (having the σ lone pair as HOMO) explains why the Pd complex is as powerful a reductant as the Ni analog.

G. COMPLEXES WITH TOTAL ELECTRON COUNT EXCEEDING 18

Diamagnetic TBP complexes of Ni(II) containing weak halide coligands have a low LUMO ($3a_1$), the HOMO-LUMO gap being certainly lower that in Fig. 2. One or two electrons can successively enter the σ^* LUMO via a chemical or electrochemical reduction. The structural consequence is a progressive elongation of both σ axial bonds. However, the Ni–X linkage is also subject to π type repulsions and it may be preferentially weakened. This was experimentally shown by the TBP structure of the unusually stable 19e complex (np_3)NiI [52], with a long Ni–I separation of 3.018(3) Å. Upon addition of a second electron, the iodide ligand is swept away, and it is true that, upon crystallization, the (np_3)Ni(0) complex is obtained. However, within the time scale of fast cyclic voltammetry, even the 20e anion $[(np_3)NiI]^-$ seems to have a finite lifetime as a TBP complex regardless of the very long Ni–I distance. This is shown by the reversibility of the redox process and the easy reformation of the d^9 and d^8 species. In a recent paper [53], the relation between structure, electrochemistry and electronic features of these unusual 18–20

electron species was described in detail and compared with the pp_3 analogs (the ligand pp_3 is conceptually derivable from np_3 upon replacement of the central amine with a fourth phosphine donor). In the latter case, the $3a_1$ LUMO is forced by the axial phosphine to stay at a high energy and no 19e TBP species is obtainable. Anyway, an electrochemical reduction occurs to yield the 17e TP $[(pp_3)Ni]^+$ [54] species in agreement with the depression of $3a_1$ upon the removal of iodide.

Finally, it is worth mentioning that the relative stability of 19e $(np_3)NiX$ species helps to clarify the unusual reactivity promoted by $(np_3)Ni(0)$ over organic substrates, namely the homolytic cleavage of the C–Cl bond of chlorobenzene (see eqn. (1)) [55].

$$(np_3)Ni + PhCl \rightarrow (np_3)NiCl + Ph\cdot \quad (1)$$

If a hypothetical adduct is initially formed containing the linear atomic sequence N–Ni–Cl–C, it cannot be excluded that five of the six electrons available for the axial bonding network are trapped within the axial $1a_1$–$3a_1$ MOs of the complex $(np_3)NiCl$ while a phenyl radical is released.

H. PSEUDO-TETRAHEDRAL (PT) (np_3)ML COMPLEXES

When the L_{ax} ligand trans to the amine is a relatively weak donor, the full population of the axial MO orbital ($3a_1$) can induce M–L_{ax} cleavage, as just seen in the cases above. Alternatively, the M–N bond is broken. The PT structures at the upper left corner of Fig. 1 are examples of the latter type. As seen in Table 2, the M–N distances vary in the range 3.07(1)–3.49(1) Å and, given the non-bonding character, the spread is hard to justify. Conerning the $(np_3)M$ fragment, the elongation of the M–N bond coincides with the depression of the z^2-based level below the 2e set. While the a_1 level in question approaches the energy of the 1e set, to reform the t_{2g} orbitals for a P_3M hemioctahedron, the higher 2e orbitals become extensively hybridized (see Fig. 4). The magnified d_π character favours π backdonation provided that the coligands are well suited for it. This is the case for CO and NO^+ that easily form PT complexes with elongated $(np_3)M$ fragments ($M = d^{10}$), e.g. $[(np_3)Ni(CO)]$ (**XVI**) [5] and $[(np_3)Ni(NO)]^+$[30].

Also, the phosphorus atom from the tetrahedral P_4 molecule or from the related P_4S_3 and P_4Se_3 cages can still be attributed residual π-acceptor capabilities (see $[(np_3)Ni(P_4)]$ (**XVII**) [27] and $[(np_3)Ni(P_4X_3)]$ (**XVIII**) [28,29] to stabilize PT adducts. The π interactions are certainly not crucial in the $[(np_3)HgI]^+$ complex (**XIX**) [31] containing the π-donor iodide ligand. The filled d_π orbitals, little hybridized, remain as unused lone pairs on the metal. Interestingly, in this 20e case, the bond to be broken is M–N and not M–I, at variance with the previously reported $[(np_3)NiI]^{0,-1}$ species [52] (see Sect. G).

In general, however, the π-bonding capabilities of the $(np_3)M$ fragment are exploited and it is possible to form unusual adducts or to stabilize molecular fragments that do not exist on their own. In the binuclear species $(np_3)Co{=}S{=}$

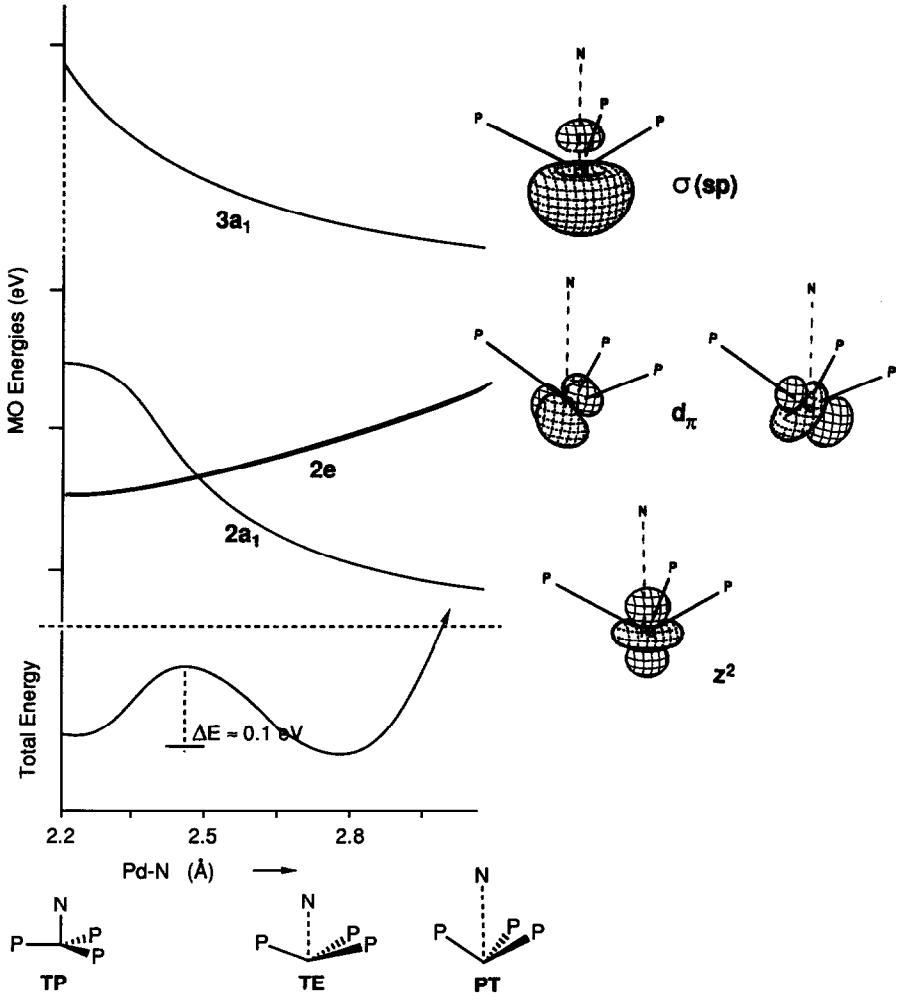

Fig. 4. Evolution of frontier orbitals for the trigonal elongation of $(np_3)Pd(0)$. The level $3a_1$ is the LUMO. Two conformational isomers, with TP and TE structures, are separated by a very small energy barrier.

$Co(np_3)$ (**XX**) [26] the multiple linear Co=S=Co bonding network (the Co–S distance is as short as 2.128(1) Å) involves the frontier FMOs typical of L_3M fragments with C_{3v} symmetry [32]. The latter, a σ(sp) and two d_π hybrids, appear in Fig. 4. By excluding active amine participation in bonding, as confirmed by the comparable structure of $[(triphos)Ni{=}S{=}Ni(triphos)]^{2+}$ [26], each metal has an apparent 16e configuration. The originally emphasized aspect of a diamagnetic Ni(II) centre having tetrahedral geometry appears rational if the sulphur atom is taken as a six-electron donor. An MO study [56] has shown that in addition to the two distinct M–S σ-type interactions, there are two π-type M–S–M interactions (three centre/two electron bonds). In this light, the proposal [57] of a total of six bonds departing

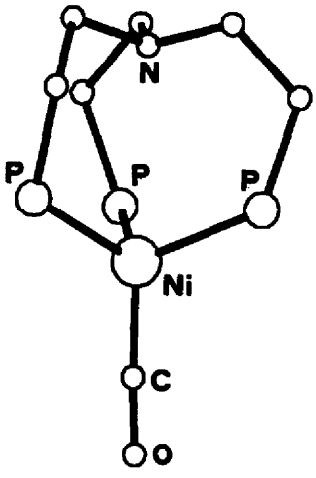

XVI

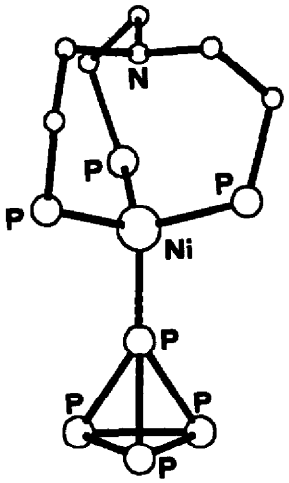

XVII

from the sulphur atom does not seem appropriate. The participation of sulphur d orbitals in bonding has stabilizing effects but is not essential.

The d_π metal orbitals of the $(np_3)M$ fragment with C_{3v} symmetry are involved in bonding small molecules or fragments in a poly-hapto coordination. An example is the complex $(np_3)Co(\eta^2\text{-SCNPh})$ (**XXI**) [25], where a C=S double bond of the heteroallenic molecule donates an electron pair to the metal and receives backdonation from the $d_{\pi_\parallel}$ orbital (lying in the SCN plane). The presence of a single electron in the orbital $\pi_\perp$ ($M = d^9$) has no major distortional effects as the degeneracy of the 2e set is removed through an in-plane π interaction with C = S. For a d^{10} metal, the

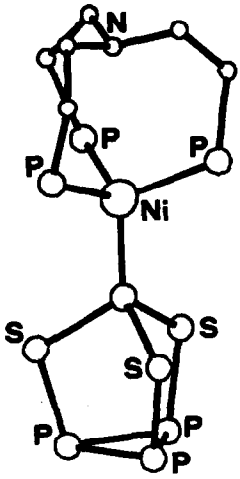

XVIII

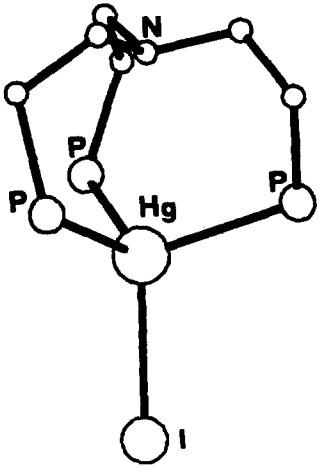

XIX

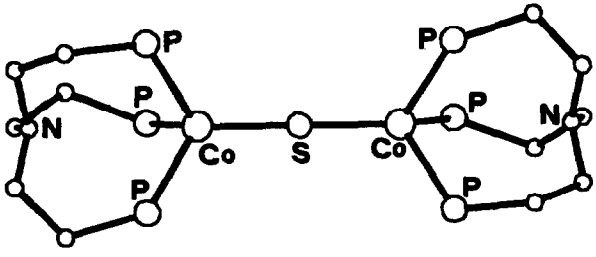

XX

$\pi_\perp$ orbital assumes the nature of a lone pair as found in a series of almost isostructural complexes of the type $L_3M(\eta^2\text{-SCS})$ [58].

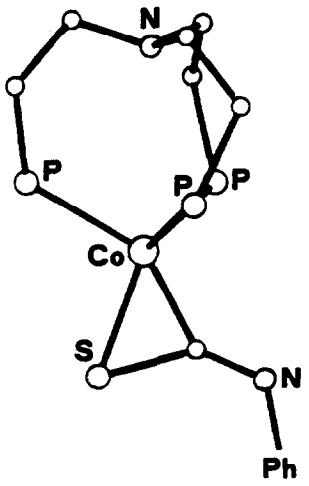

XXI

Three-hapto coordination is achieved by $(np_3)M$ fragments in the complex $(np_3)Co(\eta^3\text{-}P_3)$ (**XXII**) [24]. This species, together with the triphos analog [59], represents an astonishing example of how (tripod)M fragments can stabilize very unstable units, such as cyclotriphosphorus. Again, all the frontier FMOs of P_3M (one σ and two d_π) are fully involved in binding the $p_{\pi_\perp}$ orbitals of the P_3 unit. The chemistry and the electronic features of these compounds have been extensively reviewed [60].

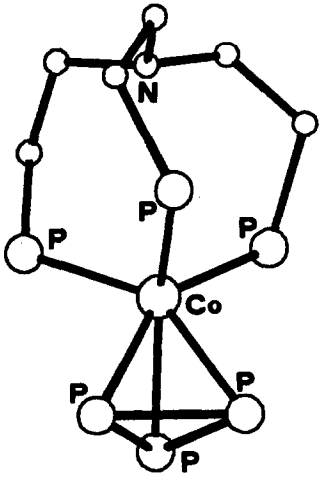

XXII

Before closing this section, it is worth noticing that in the PT complexes, where the M–N interaction seems lost, the amine group is quite flattened so as almost to retract the lone pair (the angles C–N–C range from 113 to 116°). However, the structure of the compound $[(np_3H)Ni(CO)]^+$ (**XXIII**) [61], shows that the basicity of the uncoordinated amine remains high and still points toward the metal. In fact, the complex in question is simply described as the PT species $[(np_3)Ni(CO)]$ (see **XVI**) protonated at the nitrogen atom, the proton being inside the cavity of the $(np_3)M$ fragment.

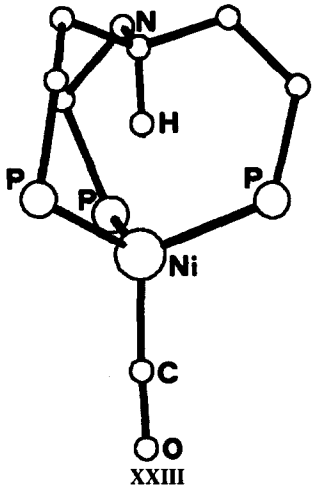

XXIII

Aside from the unexpected structural feature the way in which $[(np_3H)Ni(CO)]^+$ is formed is most interesting, namely the attack of carbon monoxide on the TBP d^8 hydride $[(np_3)NiH]^+$. A theoretical analysis of the migration of the hydrogen across the P_3Ni plane and the consequent metal reduction has previously been discussed [61].

I. INTERCONVERSION BETWEEN TP AND BUTTERFLY $(np_3)M$ FRAGMENTS. CONTROL OF THE GEOMETRY OVER OXIDATIVE ADDITION/REDUCTIVE ELIMINATION PROCESSES

A recent development of np_3 metal chemistry relates the capability of certain d^8 $(np_3)M$ fragments (similarly to $(pp_3)M$ analogs) to control basic organometallic processes such as oxidative addition and reductive elimination. Among the classical examples of the latter processes, we recall the dichotomy between classical and non-classical dihydrogen complexes, the C–H activation and the two extreme modes of olefin coordination, namely simple addition and metallo-cyclopropane [62]. In comparison with the behaviour of the related pp_3 ligand, np_3 effectively promotes the cleavage of the H–H, C–H σ bonds as well as of the π component of C=C or C=S linkages. In the light of much experimental data, including X-ray structures, it is now

clear that the geometry of the (tripod)M fragment is a critical governing parameter for chemical reactivity.

Selected $(np_3)M$ fragments ($M = d^8$) with no coligand can have a finite lifetime. The complex $[(np_3)Co]^{+9}$ has been isolated and structurally characterized (**XIII**), but its reactivity is inhibited by its triplet ground state. Potentially reactive diamagnetic d^8 species can exist in solution if the $2a_1$FMO of the TP fragment (Fig. 2) is significantly higher than 2e. In any event, the unsaturated 16e fragment is expected to distort from C_{3v} (second-order Jahn–Teller effect) with relatively little energy cost.

In the structure of the $[(np_3)IrH(\sigma\text{-}C_8H_{11})]^+$ complex (**XXIV**) [63], a result of C–H activation on cyclooctadiene, one P–M–P angle is opened up to 157.3(1)°. Analogous features are presented in the hydride acetylide complex $[(np_3)RhH(\sigma\text{-}C{=}CH)]^+$ [64]. The two complexes compare well with $[(np_3)CoCl_2]^+$ [65] (**XXV**), the closest to an octahedron with one P–Co–P angle of 166.5(5)°. In all cases, the metal is formally d^6 but the effective electron density at the metal will be low in the presence of two highly electronegative ligands such as chloride. In other words, the more oxidized the metal, the wider is one P–M–P angle. Accordingly, the latter appears to be a major governing parameter for the dichotomy reductive elimination/oxidative addition.

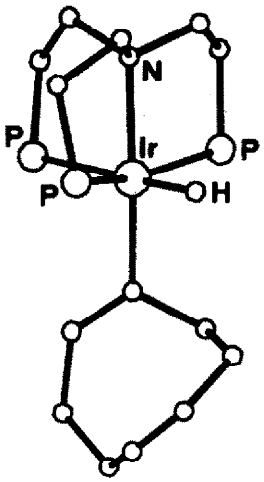

XXIV

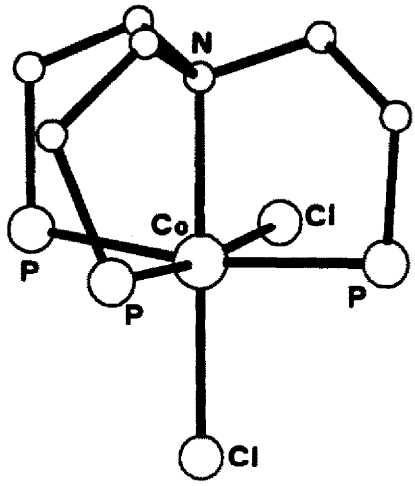

XXV

Figure 5 shows evolution of the frontier orbitals for a model of $[(np_3)Rh]^+$ in the P–Rh–P range 120–180°. At TP geometry (C_{3v}), the starting FMOs are the well-known 1e, 2e, $2a_1$ (Fig. 2). The metal has an acidic σ level ($2a_1$) and its π-bonding capabilities are limited to the xz and yz orbitals that lie unhybridized at low energy (1e). In this case, the fragment can only support a simple addition (say a dihapto coordination of an ethylene molecule) similar to Zeise's salt [62]. The recently determined structure of $[(np_3)Rh(\eta^2\text{-}C_2H_4)]^+$ (**XXVI**) [66] agrees only in part with the latter model. In fact, the coordination is close to TBP but the midpoint of the

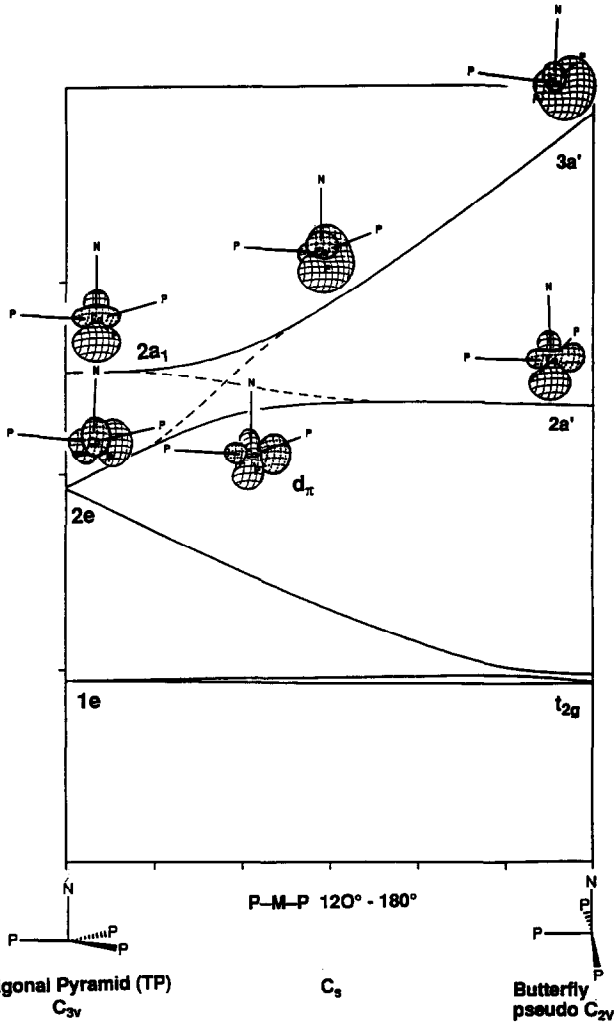

Fig. 5. A Walsh diagram relative to the opening of one P–M–P angle (range 120–180°) in the model of the fragment $[(np_3)Rh]^+$ (TBP/butterfly interconversion). The level 2a' acquires metal d_π backdonating capabilities upon an avoided crossing with 3a' (P–M–P angle ca. 140°).

olefin molecule is not exactly on the threefold axis but shifted (ca. 15°) toward the bisector of the N–Rh–P_1 angle. Such an asymmetry is unique for coordinated olefins and seems to have an unusual electronic origin, which is discussed elsewhere [66]. In any event, the most regular TBP geometry is not energetically far off, as suggested by NMR studies in solution. It is evident from the latter that the ethylene molecule can freely rotate in a position (one TBP apex) that allows equivalence of the three phosphine donors.

By opening the P–M–P angle of the $(np_3)M$ fragment, the x^2-y^2 and xy orbitals

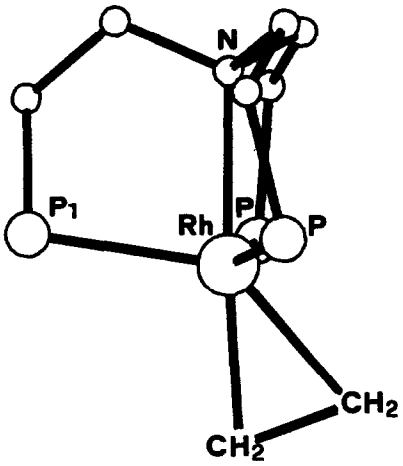

XXVI

(members of 2e) are split because the P lone pairs move from the node of the former into the node of the latter. The higher level $2a_1$ (z^2-based) should remain constant but, since the symmetry is only C_s, it undergoes an avoided crossing with the rising x^2-y^2 level. Three-dimensional drawings of the 3a′ and 2a′ levels (see Fig. 5) show that, while the former maintains its essential σ features (the empty σ-lobe is reoriented by 45°), the latter ultimately develops d_π character thanks to the mixing between x^2-y^2 and z^2. For a P–M–P angle of 180°, the frontier FMOs, typical of a butterfly fragment with pseudo-C_{2v} symmetry [55] (empty σ + filled π for $M = d^8$) are most suited to promote oxidative addition. In principle, the latter process can occur at an even earlier stage of $(np_3)M$ deformation. It is evident from Fig. 5 that, while for P–M–P values of 120–130°, the 2a′ MO still appears as an x^2-y^2 oribtal, the same level is already a d_π hybrid for angles somewhat larger than 140°. Noticeably, in the ethylene adduct (**XXVI**), the angle is just 140° whereas the values, reported above for cases of oxidative addition, are ca. 15–25° larger.

Another recent development in np_3 chemistry is provided by the documented examples of reductive elimination or of the inverse oxidative addition occurring in the solid state [67]. Under these circumstances, it is difficult to think of major conformational rearrangements, rather the fact is consistent with the dramatic change of bonding capabilities occurring within a small variation of the governing P–M–P angular parameter.

The ligand np_3 is more capable than pp_3 in promoting oxidative addition. Conversely, the latter stabilizes simple addition products or favours the process of reductive elimination. Also, this different behaviour can be qualitatively understood by looking at Fig. 5. In fact, the strength of the central donor in the tripod determines the initial energy gap between the $2a_1$ and 2e levels at TP geometry. For the amine ligand, the gap is not large and as the P–M–P angle starts to open, the avoided

crossing (with x^2-y^2/z^2 mixing) occurs quickly. By contrast, larger deformations are required for $(pp_3)M$ fragments to develop the hybridized σ and π FMOs that eventually promote oxidative addition.

APPENDIX

All of the MO calculations were of the extended Hückel type [45]. The $(np_3)M$ fragment was simulated by the model $(NH_3)(PH_3)_3M$. Unless varied to construct Walsh diagrams, the M–N and M–P distances were taken from the related crystal structures. The geometry of the various coligands was as close as possible to the experimental one. The atomic parameters for Ni, Co, Rh, Pd, P, N, Cl, S, O, C, H were the same as those used in the previous theoretical work referenced throughout the paper.

ACKNOWLEDGEMENT

This work was partially supported by the Progetto Finalizzato CNR, Chimica Fine II.

REFERENCES

1 L. Vaska and J.W. Diluzio, J. Am. Chem. Soc., 84 (1962) 679.
2 L. Sacconi and I. Bertini, J. Am. Chem. Soc., 90 (1968) 5443.
3 Cambridge Crystallographic Data Centre, University Chemical Laboratory, Lensfield Road, Cambridge CB2 1EW, UK. Copyright 1988.
4 C. Bianchini, D. Masi, C. Mealli, A. Meli, M. Sabat and G. Scapacci, J. Organomet. Chem., 273 (1984) 91.
5 C.A. Ghilardi, A. Sabatini and L. Sacconi, Inorg. Chem., 15 (1976) 2763.
6 (a) L. Sacconi, C.A. Ghilardi, C. Mealli and F. Zanobini, Inorg. Chem., 14 (1975) 1380. (b) P. Stoppioni and P. Dapporto, Cryst. Struct. Commun., 8 (1979) 15.
7 C.A. Ghilardi, S. Midollini and S. Moneti, J. Chem. Soc. Chem. Commun., (1981) 865. F. Cecconi, C.A. Ghilardi, S. Midollini and S. Moneti, J. Chem. Soc. Dalton Trans., (1983) 349.
8 M. Di Vaira and L. Sacconi, J. Chem. Soc. Dalton Trans., (1975) 493.
9 L. Sacconi, A. Orlandini and S. Midollini, Inorg. Chem., 13 (1974) 2850.
10 C.A. Ghilardi, S. Midollini and L. Sacconi, Inorg. Chem., 16 (1977) 2377.
11 S. Midollini, A. Orlandini and L. Sacconi, J. Organometal. Chem., 162 (1978) 109.
12 L. Sacconi, P. Dapporto, P. Stoppioni, P. Innocenti and C. Benelli, Inorg. Chem., 16 (1977) 1669.
13 P. Dapporto and L. Sacconi, J. Chem. Soc. A, (1970) 1804.
14 C. Bianchini, D. Masi, A. Meli and M. Sabat, Organometallics, 5 (1986) 1670.
15 P. Stoppioni, P. Dapporto and L. Sacconi, Inorg. Chem., 17 (1978) 718.
16 C. Mealli, A. Orlandini, L. Sacconi and P. Stoppioni, Inorg. Chem., 17 (1978) 3020.
17 F. Cecconi, C.A. Ghilardi, S. Midollini, S. Moneti, A. Orlandini and G. Scapacci, J. Chem. Soc. Dalton Trans., (1989) 211.
18 C.A. Ghilardi, S. Midollini, S. Moneti, A. Orlandini and J.A. Ramirez, J. Chem. Soc. Chem.

Commun., (1989) 304.
C.A. Ghilardi, S. Midollini, S. Moneti, A. Orlandini, G. Scapacci and A. Traversi, J. Chem. Soc. Dalton Trans., (1990) 2293.
19 F. Cecconi, C.A. Ghilardi, S. Midollini, S. Moneti, A. Orlandini and G. Scapacci, Inorg. Chim. Acta, 189 (1991) 105.
20 C.A. Ghilardi, S. Midollini, S. Moneti, A. Orlandini, G. Scapacci and D. Dakternieks, J. Chem. Soc. Chem. Commun., (1989) 1686.
21 F. Cecconi, C.A. Ghilardi, S. Midollini, S. Moneti, A. Orlandini and G. Scapacci, J. Chem. Soc. Chem. Commun., (1990) 1583.
22 M. Di Vaira, M. Peruzzini and P. Stoppioni, Inorg. Chem., 28 (1989) 4614.
23 C.A. Ghilardi, C. Mealli, S. Midollini and A. Orlandini, Inorg. Chem., 24 (1985) 164.
24 F. Cecconi, P. Dapporto, S. Midollini and L. Sacconi, Inorg. Chem., 17 (1978) 3292.
25 C. Bianchini, D. Masi, C. Mealli and A. Meli, Inorg. Chem., 23 (1984) 2838.
26 C. Mealli, S. Midollini and L. Sacconi, Inorg. Chem., 17 (1978) 632.
27 P. Dapporto, S. Midollini and L. Sacconi, Angew. Chem. Int. Ed. Engl., 18 (1979) 469.
28 M. Di Vaira, M. Peruzzini and P. Stoppioni, J. Organomet. Chem., 258 (1983) 373.
29 M. Di Vaira, M. Peruzzini and P. Stoppioni, Inorg. Chem., 22 (1983) 2196.
30 M. Di Vaira, C.A. Ghilardi and L. Sacconi, Inorg. Chem., 15 (1976) 1555.
31 C.A. Ghilardi, S. Midollini and A. Orlandini, to be published.
32 T.A. Albright, J.K. Burdett and M.-H. Whangbo, Orbital Interactions in Chemistry, Wiley, New York, 1983.
33 F. Cecconi, C.A. Ghilardi, S. Midollini and A. Orlandini, J. Chem. Soc. Dalton Trans., (1992) 33.
34 L. Sacconi and M. Di Vaira, Inorg. Chem., 17 (1978) 810.
35 L. Sacconi, M. Di Vaira and A. Bianchi, J. Am. Chem. Soc., 92 (1970) 4465.
M. Di Vaira and A. Bianchi Orlandini, Inorg. Chem., 12 (1973) 1292.
36 M. Di Vaira, J. Chem. Soc. Dalton Trans., (1975) 1575.
37 C. Mealli, P.L. Orioli and L. Sacconi, J. Chem. Soc. A, (1971) 2691.
38 M. Di Vaira, S. Midollini and L. Sacconi, Inorg. Chem., 16 (1977) 1518.
39 C. Bianchini, P. Innocenti, D. Masi, A. Meli and M. Sabat, Organometallics, 5 (1986) 72.
40 P. Dapporto and P. Stoppioni, Cryst. Struct. Commun., 7 (1978) 375.
41 P. Dapporto, P. Stoppioni and P.M. Maitlis, J. Organomet. Chem., 236 (1982) 273.
42 C.A. Ghilardi, S. Midollini, S. Moneti and A. Orlandini, Inorg. Chim. Acta, 42 (1991) 1.
43 C.A. Ghilardi and L. Sacconi, Cryst. Struct. Commun., 4 (1975) 687.
44 J.K. Burdett and T.A. Albright, Inorg. Chem., 18 (1979) 2112.
J. Reinhold, Z. Phys. Chem., 3 (1987) 599.
R.G. Pearson, Inorg. Chem., 12 (1973) 712.
45 R. Hoffmann, J. Chem. Phys., 39 (1963) 1397.
R. Hoffmann and W.N. Lipscomb, J. Chem. Phys., 36 (1982) 2179, 2872.
R. Hoffmann, H. Fujimoto, J.R. Swenson and C.C. Wan, J. Am. Chem. Soc., 95 (1973) 7644.
R. Hoffmann and H. Fujimoto, J. Phys. Chem., 78 (1974) 1167.
46 A.R. Rossi and R. Hoffmann, Inorg. Chem., 14 (1975) 365.
47 C. Mealli and D.M. Proserpio, J. Chem. Educ., 67 (1990) 399.
48 R. Hoffmann, Acc. Chem. Res., 4 (1971) 1.
49 R.R. Ryan, G.J. Kubas, D.C. Moody and P.G. Eller, Struct. Bonding (Berlin), 46 (1981) 47.
50 C. Mealli and L. Sacconi, J. Chem. Soc. Chem. Commun., (1973) 886.
51 C.A. Ghilardi, S. Midollini, S. Moneti and A. Orlandini, J. Chem. Soc. Chem. Commun., (1986) 1771.
52 P. Dapporto and L. Sacconi, Inorg. Chim. Acta, 39 (1980) 61.

53 C.A. Ghilardi, C. Mealli, S. Midollini, A. Orlandini, D.M. Proserpio, A. Cinquantini and P. Zanello, Struct. Chem., 1 (1990) 441.
54 F. Cecconi, S. Midollini and A. Orlandini, J. Chem. Soc. Dalton Trans., (1983) 2263.
55 P. Stoppioni, A. Biliotti and R. Morassi, J. Organomet. Chem., 236 (1982) 119.
56 C. Mealli and L. Sacconi, Inorg. Chem., 21 (1982) 2870.
57 T.J. Greenhough, B.W.S. Kolthammer, P. Legzdiens and J. Trotter, Inorg. Chem., 18 (1979) 3543.
58 C. Bianchini, C. Mealli, A. Meli and M. Sabat, in I. Bernal (Ed.), Stereochemistry of Organometallic and Inorganic Compounds, Vol. 1, Elsevier, Amsterdam, 1986, p. 146.
59 M. Di Vaira, C.A. Ghilardi, S. Midollini and L. Sacconi, J. Am. Chem. Soc., 100 (1978) 2550.
60 M. Di Vaira and L. Sacconi, Angew. Chem. Int. Ed. Engl., 21 (1982) 330.
61 F. Cecconi, C.A. Ghilardi, P. Innocenti, C. Mealli, S. Midollini and A. Orlandini, Inorg. Chem., 23 (1984) 922.
62 J.P. Collman, L.S. Hegedus, J.R. Norton, R.G. Finke, Principles and Applications of Organotransition Metal Chemistry, University Science Books, Mill Valley, CA, 1987.
63 C. Bianchini, D. Masi, A. Meli, M. Peruzzini, M. Sabat and F. Zanobini, Organometallics, **5** (1986) 2557.
64 C. Bianchini, C. Mealli, M. Peruzzini, F. Vizza and F. Zanobini, J. Organomet. Chem., 346 (1988) C53.
65 M. Di Vaira, A. Meli and L. Sacconi, Cryst. Struct. Commun., 6 (1977) 727.
66 C. Bianchini and C. Mealli, to be published.
67 C. Bianchini, M. Peruzzini and F. Zanobini, Organometallics, 10 (1991) 3415.